The content of this article is identical to:
M.J. Simmonds, T. Schwarz-Selinger, M.I. Patino, M.J. Baldwin, R.P. Doerner, und G.R. Tynan.
„Reduced Defect Recovery in Self-Ion Damaged W Due to Simultaneous Deuterium Exposure during Annealing“.
Nuclear Fusion 62 (3), 036012 (2022).
https://doi.org/10.1088/1741-4326/ac4773.

Reduced defect recovery in self-ion damaged W due to simultaneous deuterium exposure during annealing

M. J. Simmonds[a], T. Schwarz-Selinger[b], M. I. Patino[a], M. J. Baldwin[a], R. P. Doerner[a], G. R. Tynan[a,c]

[a] *Center for Energy Research, UC San Diego, 9500 Gilman Dr., La Jolla, CA 92093-0417, USA*
[b] *Max-Planck-Institut für Plasmaphysik, Boltzmannstrasse 2, D-85748 Garching, Germany*
[c] *Department of Mechanical and Aerospace Engineering (MAE), UC San Diego, 9500 Gilman Dr., La Jolla, CA 92093-0411, USA*

Abstract

Deuterium (D) plasma exposure during annealing of self-ion damaged tungsten (W) is shown to exhibit reduced defect recovery when compared to annealing without D plasma exposure. In these experiments, samples were first damaged with 20 MeV W ions. Next, samples were annealed either with or without simultaneous D_2 plasma exposure. The simultaneous annealed samples were first decorated by D_2 plasma at 383 K prior to ramping up to an annealing temperature of 473, 573, 673, or 773 K and held for 1 hour with concurrent plasma exposure. The vacuum annealed samples each had a corresponding temperature history but without D_2 plasma treatment. Finally, all samples were exposed to D_2 plasma at 383 K to decorate any remaining defects. Nuclear reaction analysis (NRA) and thermal desorption spectroscopy (TDS) shows that the simultaneous plasma-exposed and annealed samples exhibited virtually no defect recovery at annealing temper-

Email address: msimmonds@eng.ucsd.edu (M. J. Simmonds)

atures of up to 673 K, and had higher D retention than found in the vacuum annealed samples. TDS results indicate that only the lowest detrapping energy defects recover at an 773 K anneal for the simultaneous plasma annealed samples, while the vacuum annealed samples showed defect recovery at all anneal temperatures. This experiment clearly demonstrates that D occupied defects can significantly reduce or eliminate defect annealing in W, and is consistent with the existence of synergistic plasma exposure/displacement damage effects in fusion-energy relevant plasma facing materials.
Keywords: Tungsten, Deuterium, Retention, Self-ion damage, Annealing, Reduction, Synergism, Defect stabilization, NRA, TDS, Sequential, Simultaneous

---

1. Introduction

Future magnetically confined fusion devices such as ITER and DEMO will need to account for tritium retention in Plasma Facing Materials (PFMs) due to both radiation safety as well as maintaining a closed tritium (T) fuel cycle [1]. These PFMs will have induced defects from 14 MeV fusion neutrons throughout the bulk that act as trap sites for tritium. In lieu of handling activated materials, proxies for neutron damage and tritium are heavy-ion damage and deuterium, respectively. The reader is referred to the guidelines for the use of heavy ions to simulate neutron damage as outlined in [2]. Some fraction of these defects are expected to be mobile and may recover while the PFMs operate at elevated temperature (i.e. defect recovery/annealing). Additionally, annealing conditions such as temperature, mobile atom concentrations, and hydrogen-occupied defect concentrations will vary as a function of depth from the PFM surface.

PFM studies are typically performed with sequential steps due to either experimental limitations, or to independently control experimental parameters, or both. As a result, synergistic plasma exposure/displacement damage effects may be missed in experiments carried out with sequential exposures unless carefully thought through exposure schemes are used. For instance, ion damage has been shown to saturate ($\sim$0.2 dpa) as measured by D retention [3]. By damaging near saturation, then decorating the defects with a D plasma exposure prior to a second ion damage step, a marked increase in defects above saturation was shown to occur [4]. That work then posited that the defects are stabilized by D presence during the second W damage dose. In light of that finding, additional experiments exploring sequential

and simultaneous schemes are needed to uncover possible synergistic effects. In particular, the effect of such synergistic processes on the annealing of displacement damage is of interest in light of the severe environment that PFMs must endure in any fusion energy system.

All studies on defect annealing show a monotonic reduction in defects with increasing temperature when performed in sequential steps: ion damage, annealing, and then D decoration [5, 6]. Simultaneous heavy ion damage and annealing (i.e. dynamic annealing) followed by a D decoration step displayed a small increase in defect recovery compared to sequential steps [7, 8, 9]. Fully simultaneous ion damage, annealing, and relatively low flux D exposure displayed reduced defect recovery compared to sequential steps [10]. Lastly, Pečovnik *et al.* [11] utilized multiple ion damage steps and D exposure steps that showed a small reduction on the subsequent defect recovery. In summary, annealing of damaged samples with D present resulted in reduced defect recovery for sample that had seen either simultaneous or prior D implantation steps.

To isolate and quantify an effect from D presence during defect annealing, the study presented here aims to maximize the D occupation of defects during annealing. Simply performing D decoration at elevated temperature would allow a population of hydrogen-free defects to anneal prior to the diffusing solute D reaching the defects. Similar to [11], this study used D_2 plasma exposure at relatively low sample temperature to decorate defects prior to the anneal step. That experiment [11] performed annealing in vacuum, allowing thermal desorption to partially depopulate D trapped in defects. In contrast, this experiment utilized a simultaneous D_2 plasma exposure during the an-

neal step to increase the D solute concentration and, in turn, increase the trapped D population present throughout the entire annealing process. As such, we argue that this experiment better reflects PFM conditions during plasma operations while vacuum annealing with previous D decoration [11] reflects the bakeout of PFMs.

Lastly, the annealing temperatures for this experiment were chosen to ensure the self-ion induced defects were at least partially populated with D during anneal. For reference, the well documented but highly disputed recovery stages of interest for annealing without D exposure are as follows: (I) $<$ 100 K free interstitial mobility, (II) 100 - 623 K trapped interstitials released and mobile, (III) 623 - 913 K mono-vacancies become mobile [12, 13]. Note that the uncertainty in the recovery stage temperature is highlighted by new work that better isolated mono-vacancy mobility to begin closer to 550 K [14, 15]. The anneal time-at-temperature of one hour was chosen based on the work by Markina *et al.* [5]. In fig. 2 of that work, the D concentration in W damaged samples annealed at 820 K was shown to saturate within $\sim$30 minutes of time-at-temperature.

2. Experiment

2.1. Sample Preparation

Nine samples of 99.95 wt.% polycrystalline W (PCW) were 1.5 mm thick and 7.5 mm in diameter on the rear-facing side with a step to 6 mm in diameter on the plasma-facing side. All samples were polished to a mirror-like finish by successive polish treatments ending with a 3 μm grit. Next, ultrasonic baths of acetone followed by ethanol removed polishing contaminants.

Samples were annealed at 1350 K for 1 hour primarily to outgas. A separate short anneal was performed from room temperature to 2000 K in ∼20 seconds and held-at-temperature for 3 minutes. The short high temperature anneal was above the recrystallization temperature, minimizing the intrinsic level of various defects throughout the sample bulk.

2.2. Self-Ion Damage

The W samples were irradiated identically, with 20.3 MeV W^{6+} ions at the TOF beamline of the tandem accelerator laboratory at Max-Planck-Institut für Plasmaphysik in Garching (IPP) while under a low vacuum of 10^{-6} Pa and held at 295 K with a water-cooled sample holder, as detailed in [16]. A stainless steel mask held the samples at the outer unpolished rim ensuring that the polished surface was homogeneously irradiated. The implanted W dose was 7.87×10^{17} ions/m^2 with an average flux of 8.7×10^{13} ions/m^2/s to achieve a peak dpa of 0.23 (Kinchin-Pease) as calculated in SRIM [17]. The majority of defects occur within the damage zone (< 2.25 μm) with the peak near 1.3 μm.

2.3. D_2 Plasma Exposure

The PISCES-E plasma device, a 13.56 MHz RF source [18], was used to expose the self-ion damaged W samples to a D_2 plasma with a neutral pressure of 0.5 Pa at various times outlined in the following anneal scheme. An RF-compensated Langmuir probe measured an average flux of 1.1×10^{21} ions/m^2/s uniformly across the surface of the sample holder as detailed in [19]. The sample holder was biased -60 V to implant D with an ion impact energy of ∼67 eV. Sample temperature was measured by a

thermocouple in rear contact and manually controlled by either air cooling or heating a resistive coil attached to the sample manipulator.

2.4. Anneal Schemes

In addition to a control sample, the annealing schemes outlined in what follows produced two distinct subsets of annealing data. The schemes can be summarized by the following naming structure. Each sequential step is labeled and separated by a "-". The labels are as follows: "W" for self-ion damage, "D" for D_2 plasma exposure, and "A" for annealing at a particular temperature. The control sample was not annealed and is labeled "W-D." The "vacuum annealed" set is labeled "W-A-D." The "plasma annealed" set is labeled "W-D-AD-D." Note that the "AD" emphasizes that the anneal and D_2 plasma exposure were performed simultaneously.

Prior to the following anneal steps, all W samples were identically prepared and self-ion damaged. One control sample (W-D) received no additional annealing. Four samples (W-A-D) were annealed under vacuum at either 473, 573, 673, or 773 K for 1 hour. Another four samples (W-D-AD-D) were first exposed to a D_2 plasma at 383 K to a fluence of 1.0×10^{25} ions/m^2 to decorate self-ion induced defects. While still under plasma, the sample temperature was increased to one of the four annealing temperatures. Held at temperature for 1 hour, these samples were exposed to an additional fluence of 4.0×10^{24} ions/m^2. Finally, all samples were exposed to plasma to an additional fluence of 2.0×10^{25} ions/m^2 at 383 K to decorate all remaining defects in the self-ion damage zone.

2.5. NRA

To measure the D depth profile, NRA was performed at IPP Garching after the final plasma exposure. Detectors positioned at a reaction angle of 175° and 102° measured protons and alphas, respectively, from the D(^{3}He,p)^{4}He nuclear reaction as well as the backscattered ^{3}He under a scattering angle of 165°. The cross-section and further details on the optimized kinematic considerations for the 175° annular proton detector are outlined in [20, 21]. A ^{3}He ion beam was used to probe the first ∼7.4 μm of D implanted in W with decreasing energies of 4.5, 3.2, 2.4, 1.8, 1.2, 0.8, 0.69, and 0.5 MeV. SimNRA and NRADC were employed to determine the most probable D concentration as a function of depth [22, 23].

2.6. TDS

To measure the temperature dependent desorption, TDS with a linear ramp rate (β = 0.05 K/s) up to 1273 K was performed at UCSD. A thermocouple in contact with the rear of the sample measured the temperature during heating with IR lamps. A quadrupole mass spectrometer (QMS) measured the partial pressures of H_2, HD, and D_2, that was converted to a surface flux using a calibrated D_2 leak bottle and assuming the D desorbed from the 6 mm diameter plasma-facing surface alone. Total D flux was calculated using both the HD and D_2 signal as previously described in Yu [24]. Note that the D_2 flux was the dominant component in all data taken.

3. Results

3.1. NRA

The NRA determined D depth profiles highlight the stark contrast between the two anneal schemes. In fig. 1 (a) and (b), the D concentration for the control (W-D) is shown with a solid black line/star and the SRIM calculated self-ion damage is shown with a dashed grey line. For the vacuum annealed (W-A-D) samples, fig. 1(a) shows a monotonic decrease in D concentration with increasing anneal temperature. For the plasma anneal (W-D-AD-D) samples, fig. 1(b) shows D concentration within the damage zone remains constant up to an anneal temperature of 673 K. Although the D concentration in the damage zone for the plasma anneal at 773 K dropped, the concentration was still higher than the vacuum anneal at the same temperature and comparable to the 573 K vacuum anneal. In addition to the higher D concentration within the damage zone, the plasma anneal has on average ten times higher D (not shown) than the vacuum anneal near the max NRA probed depth (~ 7.75 μm).

3.2. TDS

The D flux measured by TDS also produced significantly different desorption profiles for the two anneal schemes. In fig. 2 (a) and (b), the D flux for the control (W-D) is shown with a solid black line/star. The anneal temperature prior to the final D decoration is shown with vertical dash-dot lines. For the vacuum annealed samples, fig. 2(a) displays the same monotonic decrease in D flux with increasing anneal temperature as shown in the NRA data. For the plasma annealed samples, fig. 2(b) shows a marked increase in

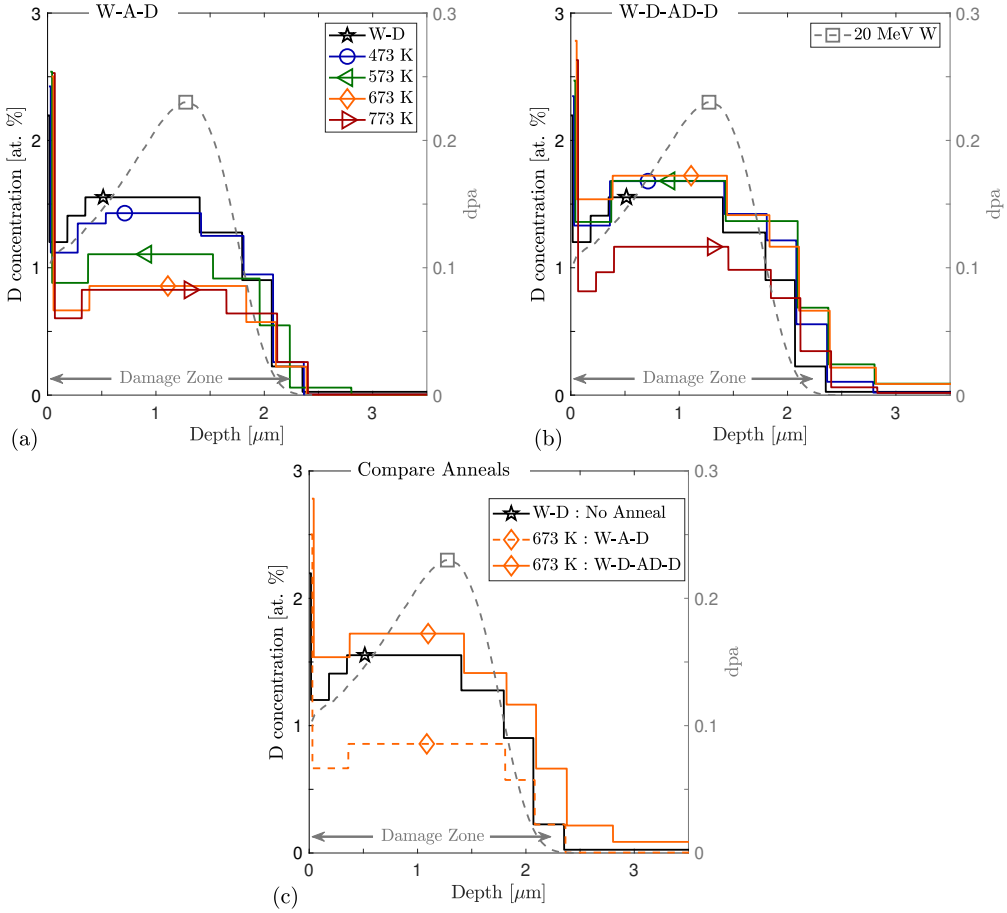

Figure 1: NRA measured D depth profiles for a control (W-D) without annealing and for annealed sample set are shown with respect to the left axis. The SRIM determined damage profile is displayed on the right axis. (a) Vacuum anneal displays a monotonic decrease in concentration. (b) Plasma anneal displays higher D concentration at all depths. (c) Direct comparison of vacuum and plasma anneal at 673 K.

D flux compared to the relatively constant D concentration seen in the NRA data.

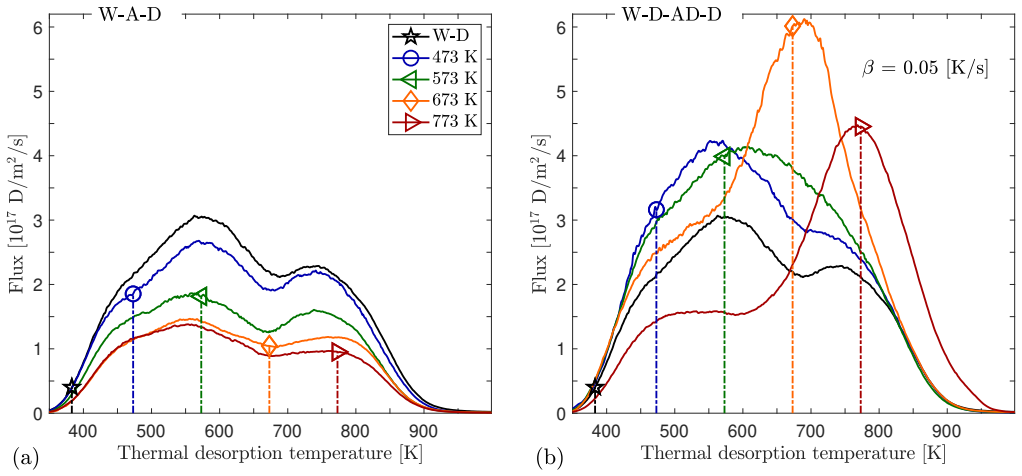

Figure 2: TDS measured D desorption flux for a control (W-D) sample without annealing and for annealed sample set are shown. The vertical dash-dot lines emphasize the sample anneal temperature. (a) Vacuum anneal displays a monotonic decrease for desorbed D. (b) Plasma anneal with D present displays much higher D release at elevated temperatures.

3.3. Retention

D retention data with respect to anneal temperature is plotted in fig. 3. Retention for NRA is determined by integrating the D concentration shown in fig. 1 over the depth. Retention for TDS is determined by integrating the D flux shown in fig. 2 over time. The plots include data from a similar experiment [11] with the same self-ion damage and comparable plasma conditions. The induced defects were decorated with D prior to a vacuum anneal step. That data is labeled using the same naming convention previously outlined in this paper by "W-D-A-D" and "W-D-W-A-D." Total D retention measured by NRA and TDS are shown with solid symbols and lines in fig. 3(a) and (b), respectively. The NRA measured retention within the damage zone is shown with open symbols and dashed lines on both figures.

Both NRA and TDS data for the vacuum anneal with empty defects (W-A-D) shows the lowest retention and thus the highest reduction in defects. Examining previously published results, the vacuum anneal with filled defects (W-D-A-D [11]) shows an increase in D retention compared to W-A-D. The plasma anneal (W-D-AD-D) retention reported here in this work is the next highest. Finally, the previously published double damage vacuum anneal with partially filled defects (W-D-W-A-D [11]) displays the highest overall retention, especially in the damage zone. Both vacuum anneals with prior D decoration show a significant reduction in retention with increasing anneal temperature, unlike the plasma anneal that showed nearly constant retention until an anneal temperature of 773 K.

Total retention can then be determined from NRA and TDS data by integrating the area under a given dataset. The results are shown in fig. 3(a) and (b) for NRA and TDS results respectively. The solid and open upward triangles for W-A-D show little difference between total and damage zone retention in fig. 3(a) and (b). In comparison, the downward triangles for W-D-AD-D showed significantly more D for total retention. This difference demonstrates that the additional D dose prior to and during annealing resulted in a significant D population between 2.25 and 7.75 μm in (a) and the bulk (> 2.25 μm) in (b). Furthermore, all other annealing conditions show little retention beyond the damage zone. Only W-D-AD-D resulted in a large difference that shows a significant amount of D diffused beyond the damage zone during the simultaneous D exposure and anneal step.

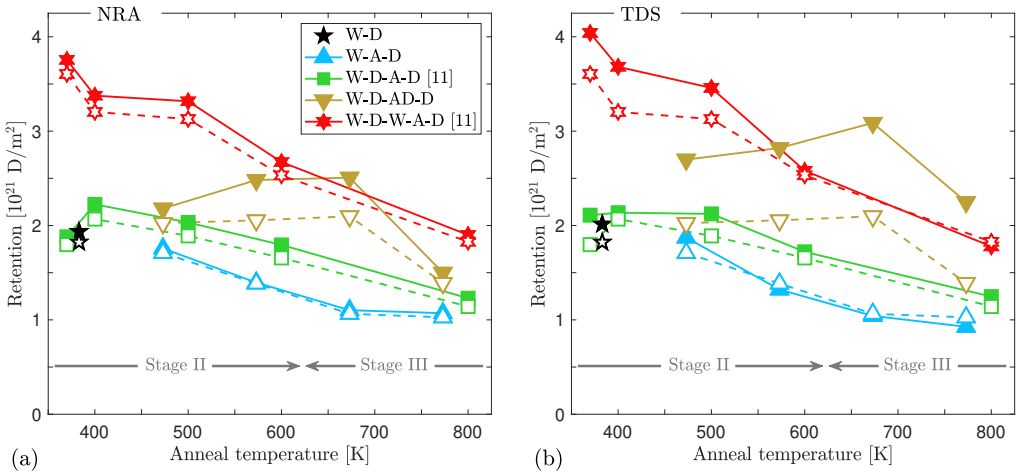

Figure 3: D retention for this experiment and Pečovnik *et al.* [11]. (a) Total D retention measured via NRA is shown with solid symbols and retention in the damage zone (< 2.25 μm) is shown with open symbols. (b) Total D retention measured via TDS is shown with solid symbols. NRA retention in the damage zone is plotted again with open symbols.

3.4. Gaussian Fit to TDS Data

As shown in fig. 5 of the Pečovnik *et al.* [11] paper, multiple detrapping energies corresponding to observed release peaks can be used to model the TDS data. That work assumed three defect types with multiple fill levels, resulting in 8 distinct release peaks used to model the measured TDS data. Utilizing the similarities between these two experiments, 8 Gaussians corresponding to the release peaks shown in that earlier work are used here to fit both sets of data. That is, since both experiments used the same damage species, energy, and dose as well as the same TDS ramp rate, the thermal desorption data are highly comparable. The main difference was a 15 K shift to lower release temperatures for TDS data shown in fig. 2 compared to [11]. Note that the temperature shift is systematic and typical when comparing

different TDS apparatus. An example of the fit for the control (W-D) is shown in fig. 4. The first 5 peaks (traps 1-5), the next 2 peaks (traps 6-7), and the last peak (trap 8) correspond to the multiple detrapping energies for the three defect types considered in [11] and further described in Section 4.1.

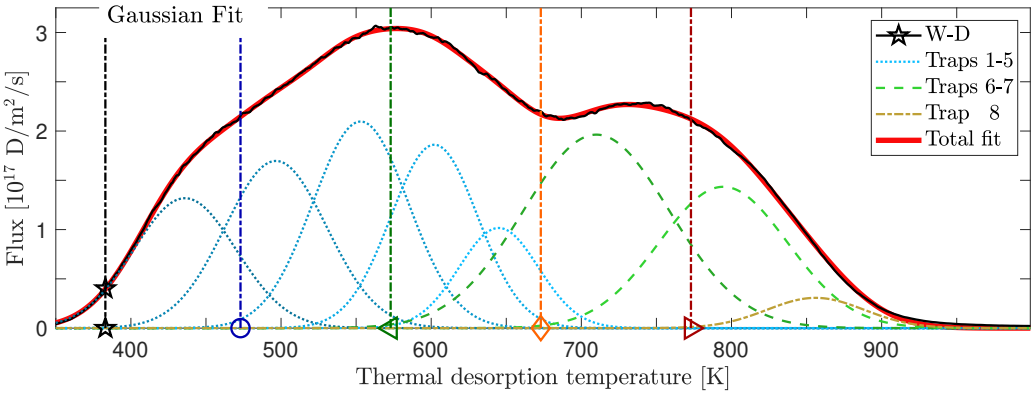

Figure 4: The control (black line) is fit (thick red) with the sum of 8 Gaussians labeled/grouped as traps 1-5 (blue), traps 6-7 (green), and trap 8 (gold). The vertical lines represent the annealing temperatures performed in this work.

The resulting D retention found in the three trap groups are plotted in fig. 5. A few markers shown are empty to represent a depopulated defect during the anneal step. It should be noted that this Gaussian fit method does not properly take into account the D released from traps further from the surface. D released from these further traps will shift the release peak to higher temperature, meaning the retention in the higher detrap energies are overestimated. Thus, the estimated eight Gaussian fit to the TDS data is not to be taken as quantitative measure. Instead, the general trend of the defects associated with each trap group give a qualitative picture of the change in defect population. The trends in defect recovery and D population are explored in the Discussion.

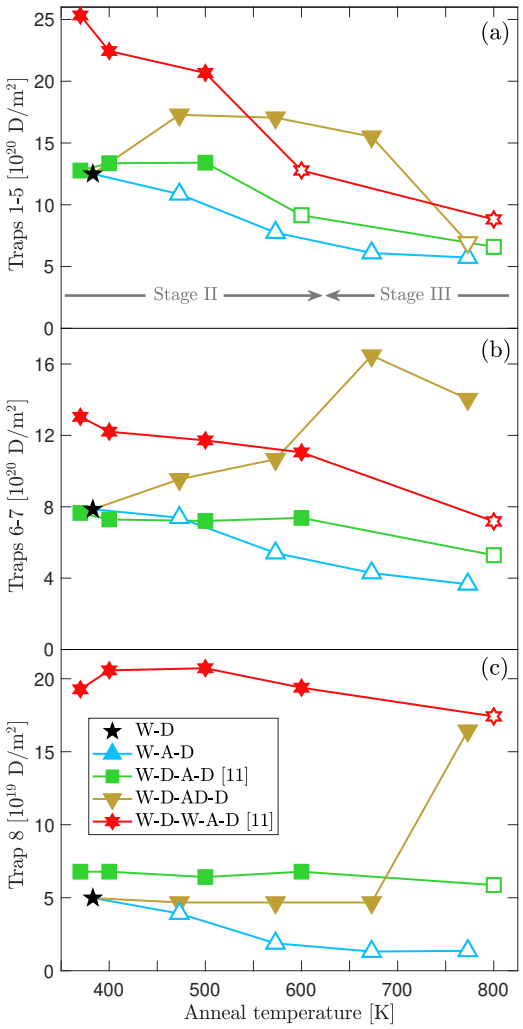

Figure 5: The result from a multiple Gaussian fit to the TDS data is plotted. Each panel presents total retention in traps 1-5 (a), 6-7 (b), and 8 (c), respectively.

3.5. Recovery

To isolate the change in D retention for the plasma anneal, fig. 6(a) and (b) plot the difference (Δ) in flux and retention with respect to the control (W-D). The differences are highlighted noting that the NRA in fig. 1(b) shows the plasma anneal and control have comparable retention in the damage zone

up to 673 K. The plot in (a) shows the growth and shift in additional D to higher temperature release. The plot in (b) illustrates the same data with respect to the retention found by performing a fit using the 8 Gaussians shown in fig. 4 and 5. In addition, the difference between D retention measured by NRA in the damage zone is also plotted with red squares. While the positive delta flux and retention denote additional defects with respect to the control, the negative values are due to defect recovery/removal. Fig. 6(a) and (b) clearly demonstrate that the only clear evidence of recovery in plasma annealing occurs for traps 1-5 at 773 K.

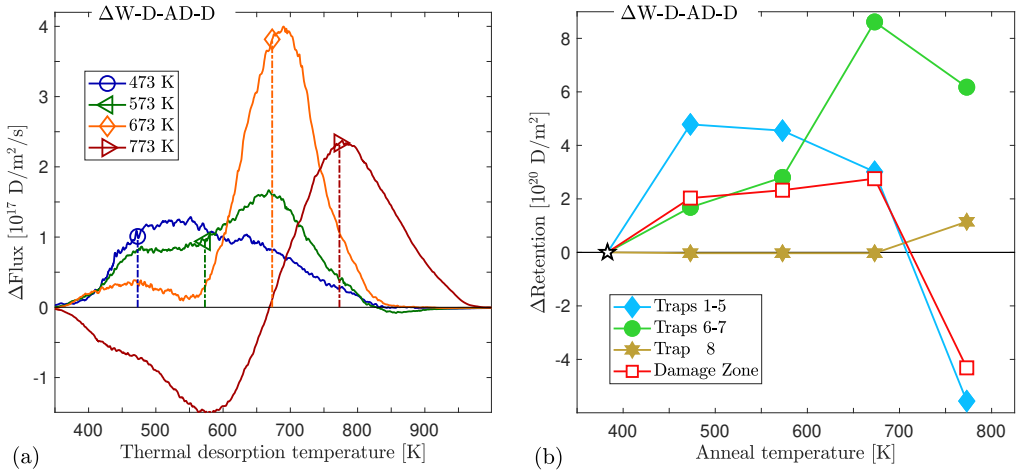

Figure 6: (a) The TDS data for W-D subtracted from W-D-AD-D at the respective anneal temperature is shown. The delta flux highlights the additional D retention and the shift to higher temperature. (b) The difference in retention for each trap group is shown for the same data in (a). The difference in retention found in the damage zone is plotted with red squares.

4. Discussion

4.1. Defect Types

Here we will restrict the discussion to three defect types corresponding to the dominant release peaks seen in the TDS data. Though there are possible overlapping detrapping energies from other defect types (e.g. dislocations and grain boundaries [25]), for simplicity we will confine the discussion to mono-vacancies (MV) and vacancy clusters (VC). Similarly to [11], here defect type 1 (traps 1-5) is thought to be primarily associated with the first five D fill levels of MV defects. Defect type 2 (traps 6-7) are thought to be associated with small VCs with two fill levels. The final release peak, defect type 3 (trap 8) is thought to be associated with a large VC with a single detrapping energy. In the rest of this section, fig. 5 is used to infer the defect evolution after annealing. From top to bottom, the panels can be interpreted as MV (a), small VC (b), and large VC (c), respectively.

4.2. Vacuum Anneal: No D present

From an anneal temperature of 473 to 773 K, all vacuum annealed (W-A-D) defects (upward triangle) monotonically decrease as expected. In stage II recovery, it is posited that the vacuum anneal reduces vacancies by thermally releasing trapped interstitials for recombination with MV and VC [12]. By stage III ($>$ 623 K), MV become mobile and may annihilate through recombination, reaching a free surface, or agglomeration. Note that for agglomeration, the addition of a single MV to a VC will decrease the total MV concentration but does not necessarily increase the VC concentration. Instead, the VC fill level and associated detrapping energies may shift slightly

higher and deeper [26]. Even at 773 K, small and large VC are not mobile, nor will they dissociate. Compared to the control, total D retention reduced by 50% at 773 K for the vacuum anneal without D present.

4.3. Vacuum Anneal: Prior D decoration

In the work presented in [11], the two vacuum anneal schemes (W-D-A-D and W-D-W-A-D) were performed after D plasma exposure filled the defects in the damage zone. Fig. 10 of [11] details the simulated D fill level after the vacuum anneal. The MV are shown to be empty at 800 K and highly depopulated at 600 K. Below 600 K, the deepest MV trap (5) remains highly populated. The small VC remain highly filled up to 600 K, but nearly empty by 800 K. The large VC are highly populated up to 600 K and only partially depopulated at 800 K. Note that for the double damage scheme, the anneal step occurred after the second damage dose without a second D decoration. The result was a small population ($\sim$5%) of empty small and large VC during the anneal step at 400 K.

Here we consider the fill population and how it may affect defect evolution during the anneal. The single damage (square) shows constant retention up to 500 K. By 600 K when the MV are highly depopulated, the retention begins to decrease nearly in parallel to W-A-D. The double damage (hex-star) does not stay constant at low anneal temperature. The drop in retention at 400 K and relatively constant retention at 500 K may be due to the initially empty population prior to the anneal step becoming populated as the weakly trapped (i.e. traps 1-4) D escapes and fills these empty traps. Similar to the single damage, by 600 K the double damage MV retention significantly decreases and also appears to decrease in parallel to W-A-D.

For the small and large VC, nearly the same story of recovery plays out for both the single and double damage, respectively. The main difference is that the temperature where recovery occurs is shifted to 800 K, the temperature at which the small VC are highly depopulated and large VC partially depopulated. Below 800 K, both VC remain highly populated and the retention remains nearly constant for the single damage scheme. For the double damage scheme, similar to the MV, some fraction of new VC may remain empty prior to annealing and account for a small amount of D retention below 600 K.

4.4. Plasma Anneal: Simultaneous D decoration

Unlike the vacuum anneals, the defects in the simultaneous plasma anneal (downward triangle) remain highly populated with D during the time-at-temperature. Fig. 4 shows the overlap of release peaks and anneal temperatures. The deepest MV trap (5) overlaps with the 673 K anneal showing that the D would significantly detrap at this temperature, yet the high D solute concentration from the concurrent plasma exposure ensures a high rate of retrapping D. The same is true for the small and large VC, as they remain highly populated at all anneal temperatures performed. By 773 K the MV are finally depopulated, as the rate of retrapping can not compete with the detrapping.

At 673 K and below, it was shown in fig. 1(b) that the D concentration in the damage zone was relatively constant. Though TDS measured a significant increase, the constant NRA retention may indicate that there was little defect evolution in the damage zone. While both the MV and small VC increased below 773 K, the additional retention is likely due to plasma

exposure induced defects in the bulk (see below). As shown in fig. 6, the only defect with evidence of recovery was MV at 773 K. At 773 K in fig. 6(b), the difference in D retention measured by NRA in the damage zone coincides with the reduction in retention for MV. Thus, the defects that remained populated with D within the damage zone are likely to have remained unchanged. Lastly, note that by 773-800 K the MV are highly depopulated and retention nearly converges for all schemes. Once again, note that these trends are qualitative since the Gaussian fit method used does not accurately account for the D trapped beyond the W damage zone.

4.5. Additional Retention

Normally in a D retention study for heavy-ion damaged W, NRA shows the majority of D is located in the damage zone. This allows for the assumption that the TDS measured D desorption is primarily detrap energy dependent and not significantly broadened/shifted to higher temperature due to spatially deeper defects in the bulk. Though the sample preparation included a high temperature anneal prior to damage to minimize intrinsic defects, the bulk displayed a high D retention for the simultaneous plasma anneal. This makes it difficult to distinguish the location of the trapped D with respect to detrapping energy. Yet the qualitative behaviour of the annealing effects can be interpreted.

As no additional heavy-ion damage was induced, only the additional plasma exposure can be responsible for increased retention within the damage zone for the plasma anneal. The increase in D retention is highlighted in fig. 6(b) as red squares. This small but consistent increase is likely due to the additional D exposure for the plasma anneal. As shown in fig. 1 of [4],

a second D exposure did slightly increase the D concentration in the damage zone. Most likely the D fill level of the traps was increased as the lower detrapping energy traps were filled to higher capacity.

A possible source of the increased D retention within the bulk has been reported in previous work by Terentyev *et al.* [27]. There it was shown that a high flux D_2 plasma (10^{24} ions/m^2/s) caused strong plastic deformation of the W lattice and propagated dislocations far into the bulk. In that case, the high flux resulted in high solute D concentration that in turn stressed the W lattice and induced defects. In this work, the initial D decoration of defects in the damage zone was followed by the plasma anneal. During that step, the continued D implantation and quick increase from 383 K to the respective anneal temperature led to significant increase in D solute concentration from D released from low detrapping energy defects. The previously trapped D acted as a veritable reservoir of D prior to releasing the floodgates. For a brief time, the increased solute D concentration may have been high enough to induce significant defect production and led to higher D concentration measured by NRA just beyond the damage zone.

4.6. Reduced Recovery

To the authors' knowledge, no other experiments have utilized the simultaneous plasma anneal scheme W-D-AD-D. As discussed in the introduction, compared to a vacuum anneal after D decoration, this scheme maximized the solute D concentration during the anneal step to increase the occupation/fill-level of defects. The recovery of defects and in turn, the reduction in D retention correlates to the absence of D from defects. That is, D filled defects appear to retard the recovery process. Since the primary recovery occurring

at these anneal temperatures is from trapped interstitial recombination with MV and VC [12], the D filled vacancies may reduce or prevent recombination. In stage III recovery, the mobility of MV coincides with the depopulation of MV. Thus, it is difficult to decouple the effect of D occupation on MV recovery. Yet the 673 K data point for plasma annealing shows a marked reduction in recovery. That is, the D retention does not significantly decrease at 673 K when MV are mobile. Though detrapping at 673 K, the continued D implantation ensures a stable D solute population to retrap and keep at least the deepest MV trap (5) filled. The stabilized retention within the damage zone for the simultaneous plasma anneal is possibly solute concentration dependent. The interplay between the concentration of defects and the aforementioned plasma parameters (e.g. surface flux and implantation energy) can determine the D solute concentration available for retrapping. The competition between detrapping and retrapping rates determine the trap occupancy and in turn, defect annealing/evolution. For example, the temperature that allows a defect to significantly depopulate D and remain depopulated may shift with plasma flux. That is, higher D plasma flux during annealing may result in higher temperature before recovery can occur. An analysis by Hodille *et al.* [28] posits this interplay also determines the formation of superabundant vacancies (SAV) in the supersaturation layer (SSL) of D plasma-loaded W.

Lastly, the synergistic effect of increased defects found in the experiments by Schwarz-Selinger *et al.* [4] and Pečovnik *et al.* [11, 29] can be compared. In those works, the additional heavy-ion damage performed after D decoration broke the saturation of D retention usually found near $\sim$0.2 dpa. The same

synergistic mechanism for reducing defect recovery may occur. During heavy-ion damage, each highly energetic W ion induces a collision cascade and in turn a thermal spike as the kinetic energy is transferred to the W lattice by atomic displacement and heat. The MV is the most common induced defect by displacing a lattice atom far enough that the atom becomes an interstitial. A high fraction of the induced MV are recombined with the free interstitials, even at room temperature and below. Yet a significant fraction of the free and highly mobile interstitials diffuse away into the bulk or reach a free surface to annihilate. In the case of a second damage dose after prior D decoration, D trapped in a vacancy (MV or VC) near a collision cascade can be liberated directly by the cascade or indirectly by the thermal spike. For the resulting empty vacancy, there is a competition between the rate of recombination with free interstitials and retrapping of D. The net effect of increased defects after the second damage dose is commensurate with D occupation retarding defect recovery, namely either trapped (II) or free (I) interstitial recombination. Indeed, we note that the DFT calculations performed by Kato *et al.* [30] show the presence of H in a MV can prevent recombination when a self-interstitial is near.

5. Summary

Vacuum (W-A-D) and plasma (W-D-AD-D) anneal schemes were performed on self-ion damaged W. Annealing with simultaneous D exposure has been shown to increase the total D retention within the damage zone and in the bulk. From the increased retention, we can infer the concentration of remaining defects is higher for the simultaneous plasma anneal.

Analysis of the data was performed under the assumption that the defects are primarily mono-vacancies, small vacancy clusters, and large vacancy clusters. Compared to the control, the vacuum anneal resulted in recovery for all defects and total retention reduced to nearly half. In turn, the plasma anneal only showed evidence of mono-vacancy recovery and only at the highest annealing temperature of 773 K. Retention within the damage zone was reduced by nearly a third at 773 K. At all other anneal temperatures, the mono-vacancies were at least partially filled with D during the anneal. The higher detrap energies for the vacancy clusters ensured the high occupancy at all anneal temperatures and no evidence of recovery. In addition, these anneal schemes were compared to another study on vacuum annealing after D decoration [11]. The similar experimental conditions in that work also provided evidence for decreased defect recovery with respect to D occupied traps. Here we speculate that the presence of D during annealing may act to retard the recovery process and result in higher overall D retention. Since fusion relevant PMI conditions will have annealing occur with D present, the increased retention observed under simultaneous plasma annealing requires further study.

6. Acknowledgments

This work was supported by U.S. Department of Energy under DE-FG02-07ER54912 and DE-SC0001999 as well as the University of California Office of Presidential Research Fund under 12-LR-237801.

7. Data Availability

The raw/processed data required to reproduce these findings cannot be shared at this time as the data also forms part of an ongoing study. Data requests and inquiries may be sent to the primary author.

References

[1] R. P. Doerner, G. R. Tynan, K. Schmid, Implications of PMI and wall material choice on fusion reactor tritium self-sufficiency, Nuclear Materials and Energy 18 (2019) 56–61.

[2] A. E521-96, Standard practice for neutron radiation damage simulation by charged-particle irradiation, Annual Book of ASTM Standards 12 (2009) 2.

[3] M. H. J. 't Hoen, M. Mayer, A. W. Kleyn, H. Schut, P. A. Z. van Emmichoven, Reduced deuterium retention in self-damaged tungsten exposed to high-flux plasmas at high surface temperatures, Nuclear Fusion 53 (2013) 043003.

[4] T. Schwarz-Selinger, J. Bauer, S. Elgeti, S. Markelj, Influence of the presence of deuterium on displacement damage in tungsten, Nuclear Materials and Energy 17 (2018) 228 – 234.

[5] E. Markina, M. Mayer, A. Manhard, T. Schwarz-Selinger, Recovery temperatures of defects in tungsten created by self-implantation, Journal of Nuclear Materials 463 (2015) 329 – 332.

[6] A. Založnik, S. Markelj, T. Schwarz-Selinger, Ł. Ciupiński, J. Grzonka, P. Vavpetič, P. Pelicon, The influence of the annealing temperature on deuterium retention in self-damaged tungsten, Physica Scripta 2016 (2016) 014031.

[7] O. V. Ogorodnikova, Y. Gasparyan, V. Efimov, J. Grzonka, et al., Annealing of radiation-induced damage in tungsten under and after irra-

diation with 20 MeV self-ions, Journal of nuclear materials 451 (2014) 379–386.

[8] S. Sakurada, K. Yuyama, Y. Uemura, H. Fujita, C. Hu, T. Toyama, N. Yoshida, T. Hinoki, S. Kondo, M. Shimada, et al., Annealing effects on deuterium retention behavior in damaged tungsten, Nuclear Materials and Energy 9 (2016) 141–144.

[9] M. J. Simmonds, Y. Q. Wang, J. L. Barton, M. J. Baldwin, J. H. Yu, R. P. Doerner, G. R. Tynan, Reduced deuterium retention in simultaneously damaged and annealed tungsten, Journal of Nuclear Materials 494 (2017) 67 – 71.

[10] S. Markelj, T. Schwarz-Selinger, M. Pečovnik, A. Založnik, M. Kelemen, I. Čadež, J. Bauer, P. Pelicon, W. Chromiński, L. Ciupinski, Displacement damage stabilization by hydrogen presence under simultaneous W ion damage and D ion exposure, Nuclear Fusion 59 (2019) 086050.

[11] M. Pečovnik, S. Markelj, M. Kelemen, T. Schwarz-Selinger, Effect of D on the evolution of radiation damage in W during high temperature annealing, Nuclear Fusion 60 (2020) 106028.

[12] M. W. Thompson, The damage and recovery of neutron irradiated tungsten, Philosophical Magazine 5 (1960) 278–296.

[13] F. Ferroni, X. Yi, K. Arakawa, S. P. Fitzgerald, P. D. Edmondson, S. G. Roberts, High temperature annealing of ion irradiated tungsten, Acta Materialia 90 (2015) 380–393.

[14] A. Debelle, M. F. Barthe, T. Sauvage, First temperature stage evolution of irradiation-induced defects in tungsten studied by positron annihilation spectroscopy, Journal of Nuclear Materials 376 (2008) 216–221.

[15] J. Heikinheimo, K. Mizohata, J. Räisänen, T. Ahlgren, P. Jalkanen, A. Lahtinen, N. Catarino, E. Alves, F. Tuomisto, Direct observation of mono-vacancy and self-interstitial recovery in tungsten, APL Materials 7 (2019) 021103.

[16] T. Schwarz-Selinger, Deuterium retention in MeV self-implanted tungsten: Influence of damaging dose rate, Nuclear Materials and Energy 12 (2017) 683 – 688.

[17] J. F. Ziegler, J. Biersack, U. Littmark, The stopping and range of ions in matter, Pergamon Press (1985).

[18] G. R. Tynan, A. D. B. III, G. A. Campbell, R. Charatan, A. de Chambrier, G. Gibson, D. J. Hemker, K. Jones, A. Kuthi, C. Lee, T. Shoji, M. Wilcoxson, Characterization of an azimuthally symmetric helicon wave high density plasma source, Journal of Vacuum Science & Technology A 15 (1997) 2885–2892.

[19] K. J. Taylor, S. Yun, G. R. Tynan, Control of plasma parameters by using noble gas admixtures, Journal of Vacuum Science & Technology A: Vacuum, Surfaces, and Films 22 (2004) 2131–2138.

[20] B. Wielunska, M. Mayer, T. Schwarz-Selinger, U. Von Toussaint, J. Bauer, Cross section data for the D (3He, p) 4He nuclear reaction from 0.25 to 6 MeV, Nuclear Instruments and Methods in Physics Research

Section B: Beam Interactions with Materials and Atoms 371 (2016) 41–45.

[21] B. Wielunska, M. Mayer, T. Schwarz-Selinger, Optimization of the depth resolution for deuterium depth profiling up to large depths, Nuclear Instruments and Methods in Physics Research Section B: Beam Interactions with Materials and Atoms 387 (2016) 103–114.

[22] M. Mayer, E. Gauthier, K. Sugiyama, U. von Toussaint, Quantitative depth profiling of deuterium up to very large depths, Nuclear Instruments and Methods in Physics Research Section B: Beam Interactions with Materials and Atoms 267 (2009) 506 – 512.

[23] K. Schmid, U. von Toussaint, Statistically sound evaluation of trace element depth profiles by ion beam analysis, Nuclear Instruments and Methods in Physics Research Section B: Beam Interactions with Materials and Atoms 281 (2012) 64 – 71.

[24] J. Yu, M. Simmonds, M. Baldwin, R. Doerner, Deuterium desorption from tungsten using laser heating, Nuclear Materials and Energy 12 (2017) 749–754.

[25] O. V. Ogorodnikova, Fundamental aspects of deuterium retention in tungsten at high flux plasma exposure, Journal of Applied Physics 118 (2015) 074902.

[26] J. Hou, X.-S. Kong, X. Wu, J. Song, C. Liu, Predictive model of hydrogen trapping and bubbling in nanovoids in bcc metals, Nature materials 18 (2019) 833–839.

[27] D. Terentyev, A. Dubinko, A. Bakaeva, G. De Temmerman, Strong subsurface plastic deformation induced by high flux plasma in tungsten, Fusion Engineering and Design 124 (2017) 405–409.

[28] E. Hodille, N. Fernandez, Z. Piazza, M. Ajmalghan, Y. Ferro, Hydrogen supersaturated layers in H/D plasma-loaded tungsten: A global model based on thermodynamics, kinetics and density functional theory data, Physical Review Materials 2 (2018) 093802.

[29] M. Pečovnik, T. Schwarz-Selinger, S. Markelj, Experiments and modelling of multiple sequential MeV ion irradiations and deuterium exposures in tungsten, Journal of Nuclear Materials 550 (2021) 152947.

[30] D. Kato, H. Iwakiri, Y. Watanabe, K. Morishita, T. Muroga, Supersaturated hydrogen effects on radiation damages in tungsten under the high-flux divertor plasma irradiation, Nuclear Fusion 55 (2015) 083019.